Inorganic Chemistry

Article

Cite This: Inorg. Chem. 2019, 58, 14145−14150

pubs.acs.org/IC

Iodine Adsorption in a Redox-Active Metal−Organic Framework: Electrical Conductivity Induced by Host−Guest Charge-Transfer

Xinran Zhang,[†] Ivan da Silva,[‡] Rodrigo Fazzi,[†,§] Alena M. Sheveleva,[†,∥] Xue Han,[†] Ben F. Spencer,[⊥] Sergey A. Sapchenko,[†,¶,▽] Floriana Tuna,[†] Eric J. L. McInnes,[†] Ming Li,[#] Sihai Yang,*[,†] and Martin Schröder*[,†]

[†]School of Chemistry, University of Manchester, Manchester M13 9PL, U.K.

[‡]ISIS Facility, STFC Rutherford Appleton Laboratory, Chilton, Oxfordshire OX11 0QX, U.K.

[§]Institute of Chemistry, Universidade de Sao Paulo, Sao Paulo, CEP 05508-000, Brazil

[∥]International Tomography Centre, Siberian Branch of the Russian Academy of Sciences and Novosibirsk State University, Novosibirsk, 630090, Russia

[⊥]School of Materials, University of Manchester, Manchester M13 9PL, U.K.

[¶]Nikolaev Institute of Inorganic Chemistry, SB RAS, Novosibirsk, 630090, Russia

[▽]Novosibirsk State University, Novosibirsk, 630090, Russia

[#]Department of Mechanical, Materials and Manufacturing Engineering, University of Nottingham, Nottingham NG7 2RD, U.K.

Supporting Information

ABSTRACT: We report a comparative study of the binding of I_2 (iodine) in a pair of redox-active metal−organic framework (MOF) materials, MFM-300(V^{III}) and its oxidized, deprotonated analogue, MFM-300(V^{IV}). Adsorption of I_2 in MFM-300(V^{III}) triggers a host-to-guest charge-transfer, accompanied by a partial (~30%) oxidation of the V^{III} centers in the host framework and formation of I_3^- species residing in the MOF channels. Importantly, this charge-transfer induces a significant enhancement in the electrical conductivity (Δ_σ = 700000) of I_2@MFM-300($V^{III/IV}$) in comparison to MFM-300(V^{III}). In contrast, no host−guest charge-transfer or apparent change in the conductivity was observed upon adsorption of I_2 in MFM-300(V^{IV}). High-resolution synchrotron X-ray diffraction of I_2@MFM-300($V^{III/IV}$) confirms the first example of self-aggregation of adsorbed iodine species (I_2 and I_3^-) into infinite helical chains within a MOF.

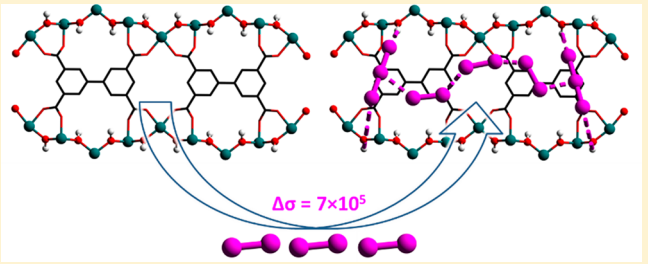

INTRODUCTION

Nuclear energy shows promise to bridge future gaps in the supply of electricity.[1] However, the radionuclides generated from the nuclear power plant can pose significant risks on both human health and ecosystems if emitted into the environment.[2] Radioactive iodine (primarily comprised of ^{129}I and ^{131}I) is a key volatile waste that can be spread through air and interferes with human metabolic processes.[3] Various techniques and materials have been applied for I_2 capture,[4,5] and porous materials, because of their high porosity and fast adsorption kinetics, are considered to be emerging sorbents for the efficient removal of I_2.

Porous solid-state sorbents with rigid structures such as zeolites, C atoms, and silica materials have been widely studied for I_2 adsorption.[6−8] Metal−organic framework (MOF) materials provide a unique platform to investigate their interaction with adsorbed I_2 because of their crystalline nature and tunable structural properties.[9] Various approaches, including linker functionalization[10] and shaping of the porosity,[11] have been reported to improve I_2 adsorption in modified MOFs. However, the binding of I_2 in MOFs with redox-active metal centers (e.g., $Fe^{II/III}$, $Cr^{II/III}$, $V^{III/IV}$, and $Ni^{II/III}$) remain largely unexplored, which can be attributed to the scarcity of reported stable redox-active MOFs.[12−15] Furthermore, collapse or, to a lesser extent, degradation of the MOF upon inclusion of I_2 can occur, thus restricting the investigation of the host−guest binding via a charge-transfer mechanism.

Herein we report the adsorption and structural study of binding domains for I_2 in a pair of stable redox-active MOFs, MFM-300(V^{III}) and MFM-300(V^{IV}).[16] Host−guest charge-transfer has been unambiguously observed in MFM-300(V^{III}) by electron paramagnetic resonance (EPR) spectroscopy, promoting a 700000 times enhancement in the electrical conductivity of the I_2-loaded MOF material in comparison to MFM-300(V^{III}). In contrast, there is an absence of host−guest charge-transfer or an apparent change in the conductivity for

Received: July 22, 2019
Published: September 30, 2019

DOI: 10.1021/acs.inorgchem.9b02176
Inorg. Chem. 2019, 58, 14145−14150

I_2-adsorbed MFM-300(V^{IV}). We also report the unusual self-aggregation of confined I_2 and I_3^- molecules into a 1D helical chain within the channels of MFM-300(V).

RESULTS AND DISCUSSION

Structure of MFM-300($V^{III,IV}$). MFM-300(V^{III}), $[V_2(OH)_2(L)]$ (H_4L = biphenyl-3,3′,5,5′-tetracarboxylic acid), crystallizes in a tetragonal system in which the V^{III} center is coordinated by six O donors, four from carboxylates and two from bridging hydroxyl groups μ_2-OH. This affords an infinite chain of $[V_2(OH)_2O_4]$ moieties along the c axis (Figure 1), and these are further bridged by the deprotonated

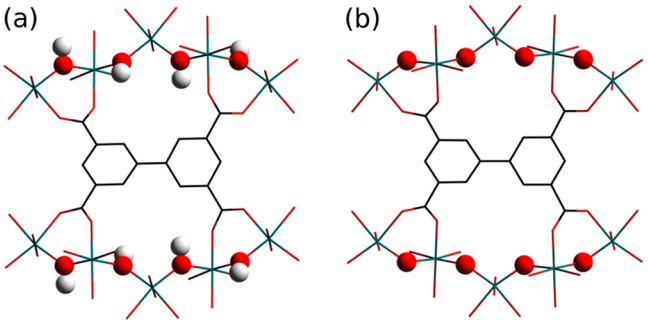

Figure 1. Views along the b axis of the infinite metal chains in (a) MFM-300(V^{III}) and (b) MFM-300(V^{IV}). The hydroxyl groups (H atom, white; O atom, red) in MFM-300(V^{III}) are deprotonated to an O^{2-} bridge (red) in MFM-300(V^{IV}).

organic linkers to afford a rigid wine-rack-type open framework with square-shaped channels of ~6.7 Å diameter. Oxidation of MFM-300(V^{III}) in air yields the analogue MFM-300(V^{IV}), $[V_2(O)_2(L)]$, where the V^{III} center is oxidized to V^{IV}, and this is coupled with deprotonation of hydroxyl to oxy bridges. MFM-300(V^{IV}) retains the same overall framework topology except for a small contraction on the V−O bond distances accompanied by a slight decrease in the pore volume from 0.49 to 0.48 $cm^3\ g^{-1}$ upon oxidation.

Iodine Adsorption in MFM-300($V^{III,IV}$). The as-synthesized MOFs were exchanged with acetone over a period of 1 week. The desolvated samples were prepared by heating the acetone-exchanged samples under vacuum for 1 day at 150 °C until no weight loss of solvent was observed by thermogravimetric analysis (TGA). The desolvated MOF was transferred into a vessel under dry N_2 containing a vial of solid I_2. The I_2 vapor was allowed to diffuse into the desolvated MOF at 343 K for 2 days to allow full adsorption. The color of both MOF materials changed from pale green and brown for V^{III} and V^{IV} materials, respectively, to dark brown. Scanning electron microscopy (SEM) images confirm the absence of surface-adsorbed I_2 or changes in the crystal morphology upon adsorption of I_2 (Figure S3). The maximum adsorption capacities of I_2 in MFM-300(V^{III}) and MFM-300(V^{IV}) have been determined by TGA−mass spectrometry (MS) to be 1.42 $g\ g^{-1}$ and 1.25 $g\ g^{-1}$, respectively (Figure 2). The difference in the adsorption uptake is due to a slight variation in the pore volumes and window sizes. These uptakes are higher than those previously reported for redox-active MOFs, such as BOF-1[17] (0.66 $g\ g^{-1}$) and Cu[Ni(pdt)$_2$][14] (H_2pdt = pyrazine-2,3-dithiol; 0.18 $g\ g^{-1}$), and are comparable with the robust ZIF-8[18] (1.25 $g\ g^{-1}$) but lower than HKUST-1[19] (1.75 $g\ g^{-1}$), which incorporates open metal sites and a larger pore volume

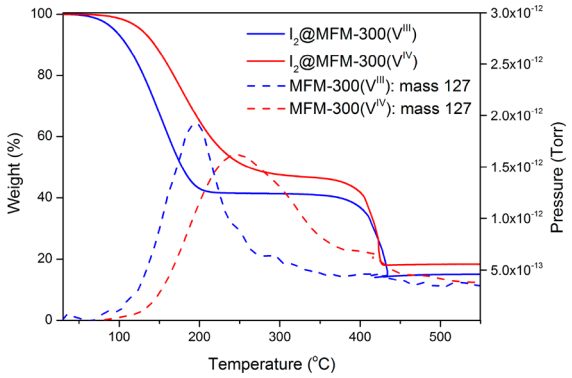

Figure 2. TGA−MS plots for I_2-saturated MFM-300(V^{III}) and MFM-300(V^{IV}).

(0.74 $cm^3\ g^{-1}$). The adsorption of I_2 in MFM-300(V) materials is fully reversible, and no apparent loss in capacity was observed for three cycles of sorption−desorption in both MOFs (Figures S4−S6). The densities of adsorbed I_2 within the pores of MFM-300(V^{III}) and MFM-300(V^{IV}) are calculated to be 2.90 and 2.60 $g\ cm^{-3}$, respectively. The former is comparable to the best-behaving MOF to date [3.08 $g\ cm^{-3}$ in MFM-300(Sc)].[20]

Determination of I_2 Binding Sites within MFM-300($V^{III/IV}$). The binding sites for adsorbed I_2 molecules within MFM-300(V) have been elucidated by high-resolution synchrotron powder X-ray diffraction (PXRD). Structural analysis of I_2-loaded MOF samples at approximately 1.0 I_2/V loading via Rietveld refinement confirmed the absence of any structural phase changes and revealed formulae of $[V_2(OH)_2(L)]\cdot1.03I_2\cdot0.6I_3^-$ and $[V_2(O)_2(L)]\cdot2.2I_2$ for I_2-loaded MFM-300(V^{III}) and MFM-300(V^{IV}), respectively. Upon loading of I_2 into MFM-300(V^{III}), changes are observed in the V−O bond lengths and angles, and three independent sites for neutral I_2 molecules and one site for anionic I_3^- are observed within the channel (Figure 3a). Bond-valence-sum (BVS) calculations (Table 1) give an overall valence of 3.28 for the V center, consistent with its partial oxidation, and this is balanced by the presence of triiodide I_3^- anions. The I_3^- anion (occupancy = 0.3) is located near the hydroxyl group from the $[V^{III}O_4(OH)_2]$ moiety with a short distance [$I_3^-\cdots$H−O = 2.94(1) Å], indicating the formation of a strong hydrogen bond between the triiodide and the −OH groups. It is worth noting that protons on the hydroxyl groups cannot be conclusively located from the PXRD data, and it is likely that these protons are partially delocalized to accompany the host−guest charge-transfer. I^{II}_2 is located interstitially between two phenyl rings of neighboring ligand molecules [$I^{II}_2\cdots$phenyl ring = 4.68(1) and 5.15(1) Å] with an occupancy of 0.25. I^{III}_2 and I^{IV}_2 adopt low occupancies (0.16 and 0.10, respectively), reside in the center of the channel, and are stabilized by intermolecular interactions (Figure S10). These results confirm partial oxidation of the framework by adsorbed I_2 molecules to afford a mixed-valence I_2@MFM-300($V^{III/IV}$) material.

$[V_2(O)_2(L)]\cdot2.2I_2$ shows two primary binding domains, I′ and II′, with occupancies of 0.59 and 0.51, respectively, for adsorbed I_2 molecules within the channel. There is little difference on the V−O bond distances in MFM-300(V^{IV}) upon adsorption of I_2, suggesting the absence of host−guest charge-transfer. Also, there is an absence of direct binding of adsorbed I_2 molecules with the pore interior such as the oxy bridges [$I_2^{I'}\cdots O_{bridge}$ = 5.67(1) Å; $I^{II'}{}_2\cdots O_{bridge}$ = 5.22(1) Å]. A

DOI: 10.1021/acs.inorgchem.9b02176
Inorg. Chem. 2019, 58, 14145−14150

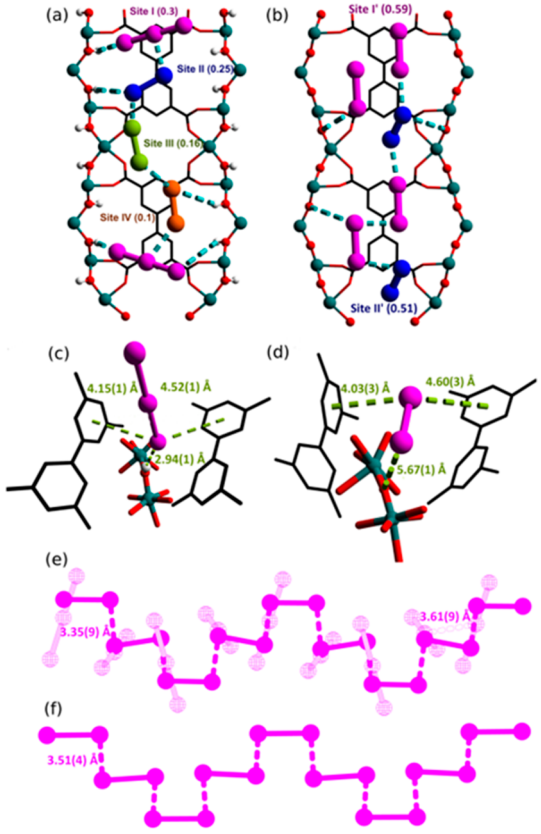

Figure 3. Views along the *b* axis of I_2-loaded (a) MFM-300(V^{III}) and (b) MFM-300(V^{IV}) obtained by high-resolution synchrotron PXRD. Views of binding sites for I_3^- and I_2 in (c) MFM-300(V^{III}) and (d) MFM-300(V^{IV}), respectively. Views of I_2 (solid) and I_3^- (pale wire frame) in (e) I_2@MFM-300($V^{III/IV}$) and (f) I_2@MFM-300(V^{IV}).

Table 1. Bond-Length and BVS Calculations of MFM-300(V^{III}), MFM-300(V^{IV}), and I_2@MFM-300($V^{III/IV}$)

	MFM-300(V^{III})	MFM-300(V^{IV})	I_2@MFM-300($V^{III/IV}$)
V−$O_{bridging}$ (Å)	1.978(1)	1.838(1)	1.901(2)
V−$O_{carboxylate}$ (Å)	2.004(2)	1.971(2)	2.014(1)
	2.007(2)	2.031(2)	2.070(9)
∠V---$O_{bridging}$---V(^{O})	125.6(1)	134.7(2)	130.1(1)
V---V distance (Å)	3.519	3.392	3.447
BVS calculation for V	3.027	3.960	3.278

detailed examination of $[V_2(O)_2(L)]\cdot 2.2I_2$ confirmed that the confined I_2 molecules within the pores aggregate to form an unusual helical chain running through the channel with a distance of 3.51(4) Å between adjacent I_2 molecules. This intermolecular $I_2\cdots I_2$ distance is comparable to that [3.35(9) Å] observed in the single helical chain of I_2 and I_3^- in I_2@MFM-300($V^{III/IV}$) (Figure 3e,f). A more detailed structural analysis of I_2@MFM-300(V^{IV}) by single-crystal X-ray diffraction reveals a similar structural model of infinite helical I_2 chains with an intermolecular $I_2\cdots I_2$ distance of 3.53(4) Å (Figure S13). To date, the existence of one-fold helical chains of I_2 has only been confirmed by theoretical studies,[21] while the linear I_2 chain has been observed crystallographically in $Ln_2Cu_5(OH)_2(pydc)_6(H_2O)_8$ (H_2pydc = pyridine-2,5-dicarboxylic acid).[22] Thus, the helical I_2 chain observed in I_2@MFM-300(V) at crystallographic resolution represents the first example of such a motif in porous materials. The formation of triple-helical I_2 chains has been previously observed in MFM-300(Sc).

Spectroscopic Analysis of I_2@MFM-300($V^{III/IV}$). X-ray photoelectron spectroscopy (XPS) was used to investigate the valence of adsorbed I_2 species within MFM-300(V) (Figure 4a,b). For I_2@MFM-300(V^{IV}), one chemical species (one doublet for the spin−orbit splitting of the 3d level) of I_2 was observed with the I $3d_{5/2}$ photoelectron peak at 620.7 eV, indicating that only one type of adsorbed I_2 species is trapped inside the pore and all of the adsorbed I_2 molecules remain neutral. For I_2@MFM-300($V^{III/IV}$), however, two characteristic chemical species (I $3d_{5/2}$ at 619.1 and 620.7 eV) were observed, corresponding to the I_3^- and I_2 moieties, respectively,[23] consistent with the structural models. Electron-accepting guest inclusion results in an increase in the electrical conductivity[24,25] so measurements of the electrical conductivity of the bare and I_2-loaded MFM-300(V) materials were performed to examine the effect of host−guest charge-transfer.

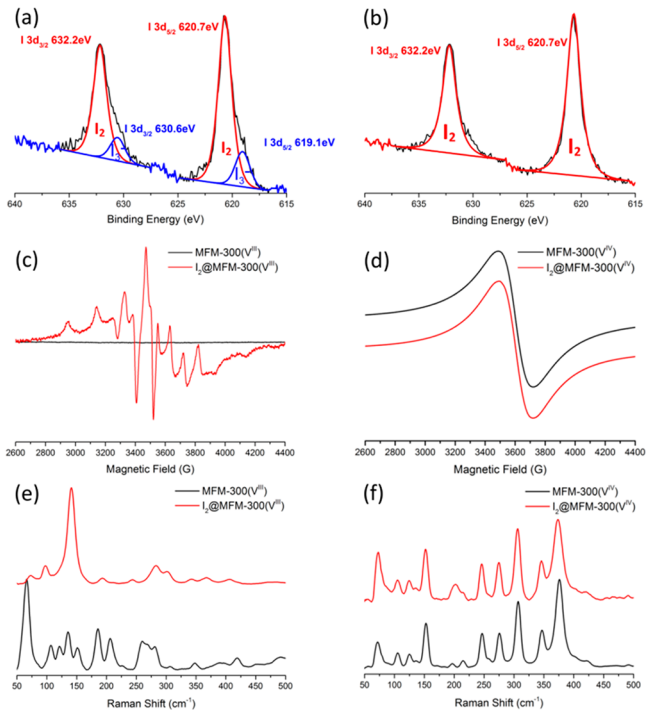

Figure 4. XPS spectra of I_2-loaded (a) MFM-300(V^{III}) and (b) MFM-300(V^{IV}). EPR spectra of desolvated and I_2-loaded (c) MFM-300(V^{III}) and (d) MFM-300(V^{IV}). Raman spectra of desolvated and I_2-loaded (e) MFM-300(V^{III}) and (f) MFM-300(V^{IV}).

The conductivity of MFM-300(V^{III}) was measured to be 1.7×10^{-10} S/cm, but I_2@MFM-300($V^{III/IV}$) shows a significant enhancement ($\Delta_\sigma = 700000$) in conductivity in the dark to 1.2×10^{-4} S/cm (Figure S14). This can be attributed to both the oxidized V−O(H)−V skeletons and generated iodide chains that provide further transport pathways to facilitate electron transfer.[26] The value is comparable to the state-of-the-art conductivity observed for I_2-loaded MOFs [1×10^{-4} S/cm for I_2@$Cu[Ni(pdt)_2]$[14] and 2.16×10^{-4} S/cm for I_2@$[Tb_3(Cu_4I_4)_3(ina)_9]_n$[27] ($H_2$pdt = pyrazine-2,3-dithiol; Hina = isonicotinic acid)] (Table 2). Measurements on MFM-300(V^{IV}) and I_2@MFM-300(V^{IV}) show very low conductivities (<1×10^{-10} S/cm) in both cases. Thus, the

DOI: 10.1021/acs.inorgchem.9b02176
Inorg. Chem. 2019, 58, 14145−14150

Table 2. Summary of Electrical Conductivities for I_2-Loaded MOFs[a]

MOF	conductivity for bare MOFs (S/cm)	conductivity for I_2-loaded MOFs (S/cm)	conductivity enhancement (magnitudes)	ref
$Cu[Ni(pdt)_2]$[b]	1×10^{-8}	1×10^{-4}	$\sim 10^4$	14
$[Cu_6(pybz)_8(OH)_2](I^-)_2$[c]	8.04×10^{-9}	8.11×10^{-7}	$\sim 10^2$	29
$[Co_{1.5}(bdc)_{1.5}(H_2bpz)]$[d]	2.59×10^{-9}	1.56×10^{-6}	$\sim 10^3$	30
$[Co(ebic)_2]_n$[d]	2.46×10^{-9}	2.21×10^{-7}	$\sim 10^2$	31
$[Eu(L^1)]$[d]	8.27×10^{-7}	2.71×10^{-5}	$\sim 10^2$	32
IFMC-15[d]	2.59×10^{-9}	2.07×10^{-7}	$\sim 10^2$	33
$\{[(Me_2NH_2)_2]\cdot[Cd_3(5\text{-tbip})_4]\}_n$[d]	1.71×10^{-8}	1.30×10^{-6}	$\sim 10^2$	34
MET-3[d]	0.77×10^{-4}	1×10^{-3}	$\sim 10^1$	35
$[Tb_3(Cu_4I_4)_3(ina)_9]_n$[c]	5.72×10^{-11}	2.16×10^{-4}	$\sim 10^8$	27
$[Zn_3(\text{D,L-lac})_2(pybz)_2]_n$[c]		$\sigma^{\parallel}=3.4 \times 10^{-3}$		9
		$\sigma_{\perp} = 1.7 \times 10^{-4}$		
$[Zn(ebic)_2]_n$[d]	4.33×10^{-9}	3.47×10^{-7}	$\sim 10^2$	31
MFM-300(V^{III})[d]	1.7×10^{-10}	1.16×10^{-4}	$\sim 10^6$	this work

[a]The value of the electrical conductivity for solid I_2 is 1×10^{-9} S/cm. H_2pdt = pyrazine- 2,3-dithiol, Hpybz = 4-pyridylbenzoic acid, H_2bdc = benzene-1,4-dicarboxylic acid, bpz = 3,3′,5,5′-tetramethyl-4,4′-bipyrazole, Hebic = 2-ethyl-1*H*-benzo[*d*]imidazole-5-carboxylic acid, H_3L^1 = biphenyl-3,4′,5-tricarboxylate, H_2-5-tbip = 5-*tert*-butylisophthalic acid, Hina = isonicotinic acid, H_2-DL-lac = lactic acid, Hpybz = 4-pyridylbenzoic acid, and Hebic = 2-ethyl-1*H*-benzo[*d*]imidazole-5-carboxylic acid. [b]Films were used for testing of the electrical conductivity. [c]Single crystals were used for testing of the electrical conductivity. [d]Pressed pellets were used for testing of the electrical conductivity.

host−guest charge-transfer in I_2-loaded MFM-300(V^{III}) enhances and promotes the electrical conductivity of the resultant mixed-valence I_2@MFM-300($V^{III/IV}$) material. Electrochemical impedance spectroscopy confirms (Figure S16) that I_2@MFM-300 ($V^{III/IV}$) with a charge-transfer resistance (R_{ct}) of 383 Ω shows higher electron conduction compared with bare MFM-300(V^{III}) with a R_{ct} value of 1112 Ω.

EPR spectroscopy confirms partial oxidation of the V centers in MFM-300(V^{III}) upon adsorption of I_2 (Figure 4c). MFM-300(V^{III}) is EPR-silent at X band, as is common for V^{III} materials because of the typically very large zero-field splitting of a d^2, $S = 1$ ion (up to tens of cm^{-1}).[16] In contrast, I_2@MFM-300($V^{III/IV}$) shows a typical V^{IV} (d^1, $S = {}^1/_2$) EPR spectrum with resolution of the ^{51}V ($I = {}^7/_2$) hyperfine interaction (Figure S15 and Table S3 for simulation and parameters). Both MFM-300(V^{IV}) and I_2@MFM-300(V^{IV}) give a broad, unresolved EPR signal (Figure 4d) consistent with V^{IV} under magnetically non-dilute conditions. Thus, the EPR spectroscopic results are entirely consistent with partial oxidation of V^{III} to V^{IV} in I_2@MFM-300($V^{III/IV}$) but a negligible effect of I_2 on the metal ions in I_2@MFM-300(V^{IV}).

Raman spectroscopy was applied to examine the nature of the interaction between adsorbed I_2 molecules and the MOF hosts. For MFM-300(V^{III}), two new peaks are observed at 150 and 185 cm^{-1} upon adsorption of I_2; the former band is prominent in the spectrum and assigned to the asymmetric stretching mode of I_3^- ions within the pores, while the latter is attributed to the vibration of neutral I_2 molecules.[28] For MFM-300(V^{IV}), in the low-energy region, a characteristic peak at 205 cm^{-1} is observed for I_2-loaded MFM-300(V^{IV}), which can be assigned to the intrinsic vibration of trapped I_2 molecules. Compared to the intramolecular I−I vibration (ca. 180 cm^{-1} for solid I_2), the blue shift ($\Delta = 25$ cm^{-1}) can be assigned to the stronger intermolecular interaction of confined I_2 molecules within the helical chains, fully consistent with the structural models derived from synchrotron X-ray diffraction data.

CONCLUSION

In summary, we report the adsorption and binding domains of I_2 in a pair of redox-active MOF materials, MFM-300(V^{III}) and MFM-300(V^{IV}), which provide an excellent platform to examine the host−guest charge-transfer properties. Adsorption of I_2 in MFM-300(V^{III}) induces host−guest charge-transfer via partial oxidation of the V centers and formation of I_3^- species in the pore to balance the overall charge. As a result, 7×10^5 enhancement of the electrical conductivity is observed for the I_2-loaded mixed-valence I_2@MFM-300($V^{III/IV}$). In contrast, there is an absence of host−guest charge-transfer observed for MFM-300(V^{IV}) upon loading of I_2 with no change in the inherent low conductivity of the parent MOF. In both cases, unusual self-aggregation of confined I_2 molecules into helical chains within the MOF hosts has been observed at crystallographic resolution, defining the molecular details for the underlying host−guest binding interactions and paving the way for the design and discovery of new functional materials with improved I_2 adsorption properties.

ASSOCIATED CONTENT

Supporting Information

The Supporting Information is available free of charge on the ACS Publications website at DOI: 10.1021/acs.inorgchem.9b02176.

Synthesis, iodine adsorption measurements, powder X-ray diffraction, SEM images, and Rietveld refinement results (PDF)

Accession Codes

CCDC 1915136−1915138 contain the supplementary crystallographic data for this paper. These data can be obtained free of charge via www.ccdc.cam.ac.uk/data_request/cif, or by emailing data_request@ccdc.cam.ac.uk, or by contacting The Cambridge Crystallographic Data Centre, 12 Union Road, Cambridge CB2 1EZ, UK; fax: +44 1223 336033.

AUTHOR INFORMATION

Corresponding Authors

*E-mail: Sihai.Yang@manchester.ac.uk (S.Y.).

DOI: 10.1021/acs.inorgchem.9b02176
Inorg. Chem. 2019, 58, 14145−14150

*E-mail: M.Schroder@manchester.ac.uk (M.S.).

ORCID

Ben F. Spencer: 0000-0002-1453-5327
Sergey A. Sapchenko: 0000-0002-2567-1594
Eric J. L. McInnes: 0000-0002-4090-7040
Sihai Yang: 0000-0002-1111-9272
Martin Schröder: 0000-0001-6992-0700

Notes

The authors declare no competing financial interest.

■ ACKNOWLEDGMENTS

We thank EPSRC (EP/I011870, EP/K038869, and EP/P001386), ERC (AdG 742041), and the Royal Society and University of Manchester for funding. We thank EPSRC for funding of the EPSRC National Service for EPR Spectroscopy at Manchester. We are especially grateful to Diamond Light Source for access to the Beamline I11. X.Z. and R.F. acknowledge financial support from China Scholarship Council and Coordenação de Aperfeiçoamento de Pessoal de Nível Superior, Brazil (CAPES), Finance Code 001, respectively.

■ REFERENCES

(1) Gralla, F.; Abson, D. J.; Møller, A. P.; Lang, D. J.; von Wehrden, H. Energy Transitions and National Development Indicators: A Global Review of Nuclear Energy Production. *Renewable Sustainable Energy Rev.* **2017**, *70*, 1251−1265.

(2) Deblonde, G. J.-P.; Ricano, A.; Abergel, R. J. Ultra-Selective Ligand-Driven Separation of Strategic Actinides. *Nat. Commun.* **2019**, *10*, 2438−2447.

(3) Oberstadt, A. E.; Nelson, N. C.; Claude, A. K.; Refsal, K. R.; Scott-Moncrieff, J. C.; Petroff, B. K.; Langlois, D. K. Radioactive Iodine Uptake in Hyperthyroid Cats after Administration of Recombinant Human Thyroid Stimulating Hormone. *J. Vet. Intern. Med.* **2018**, *32*, 1891−1896.

(4) O'dowd, C. D.; Jimenez, J. L.; Bahreini, R.; Flagan, R. C.; Seinfeld, J. H.; Hämeri, K.; Pirjola, L.; Kulmala, M.; Jennings, S. G.; Hoffmann, T. Marine Aerosol Formation from Biogenic Iodine Emissions. *Nature* **2002**, *417*, 632−636.

(5) Sava, D. F.; Garino, T. J.; Nenoff, T. M. Iodine Confinement into Metal−Organic Frameworks (MOFs): Low-Temperature Sintering Glasses To Form Novel Glass Composite Material (GCM) Alternative Waste Forms. *Ind. Eng. Chem. Res.* **2012**, *51*, 614−620.

(6) Wang, P.; Xu, Q.; Li, Z.; Jiang, W.; Jiang, Q.; Jiang, D. Exceptional Iodine Capture in 2D Covalent Organic Frameworks. *Adv. Mater.* **2018**, *30*, 1801991.

(7) Subrahmanyam, K. S.; Sarma, D.; Malliakas, C. D.; Polychronopoulou, K.; Riley, B. J.; Pierce, D. A.; Chun, J.; Kanatzidis, M. G. Chalcogenide Aerogels as Sorbents for Radioactive Iodine. *Chem. Mater.* **2015**, *27*, 2619−2626.

(8) Yan, Z.; Yuan, Y.; Tian, Y.; Zhang, D.; Zhu, G. Highly Efficient Enrichment of Volatile Iodine by Charged Porous Aromatic Frameworks with Three Sorption Sites. *Angew. Chem., Int. Ed.* **2015**, *54*, 12733−12737.

(9) Zeng, M.-H.; Wang, Q.-X.; Tan, Y.-X.; Hu, S.; Zhao, H.-X.; Long, L.-S.; Kurmoo, M. Rigid Pillars and Double Walls in a Porous Metal-Organic Framework: Single-Crystal to Single-Crystal, Controlled Uptake and Release of Iodine and Electrical Conductivity. *J. Am. Chem. Soc.* **2010**, *132*, 2561−2563.

(10) Falaise, C.; Volkringer, C.; Facqueur, J.; Bousquet, T.; Gasnot, L.; Loiseau, T. Capture of Iodine in Highly Stable Metal-Organic Frameworks: A Systematic Study. *Chem. Commun.* **2013**, *49*, 10320−10322.

(11) Marshall, R. J.; Griffin, S. L.; Wilson, C.; Forgan, R. S. Stereoselective Halogenation of Integral Unsaturated C-C Bonds in Chemically and Mechanically Robust Zr and Hf MOFs. *Chem. - Eur. J.* **2016**, *22*, 4870−4877.

(12) Brozek, C. K.; Dincă, M. Ti^{3+}-, $V^{2+/3+}$-, $Cr^{2+/3+}$-, Mn^{2+}-, and Fe^{2+}-Substituted MOF-5 and Redox Reactivity in Cr- and Fe-MOF-5. *J. Am. Chem. Soc.* **2013**, *135*, 12886−12891.

(13) D'Alessandro, D. M. Exploiting Redox Activity in Metal−organic Frameworks: Concepts, Trends and Perspectives. *Chem. Commun.* **2016**, *52*, 8957−8971.

(14) Kobayashi, Y.; Jacobs, B.; Allendorf, M. D.; Long, J. R. Conductivity, Doping, and Redox Chemistry of a Microporous Dithiolene-Based Metal-Organic Framework. *Chem. Mater.* **2010**, *22*, 4120−4122.

(15) Zeng, M. H.; Yin, Z.; Tan, Y. X.; Zhang, W. X.; He, Y. P.; Kurmoo, M. Nanoporous cobalt(II) MOF Exhibiting Four Magnetic Ground States and Changes in Gas Sorption upon Post-Synthetic Modification. *J. Am. Chem. Soc.* **2014**, *136*, 4680−4688.

(16) Lu, Z.; Godfrey, H. G. W.; da Silva, I.; Cheng, Y.; Savage, M.; Tuna, F.; McInnes, E. J. L.; Teat, S. J.; Gagnon, K. J.; Frogley, M. D.; et al. Modulating Supramolecular Binding of Carbon Dioxide in a Redox-Active Porous Metal-Organic Framework. *Nat. Commun.* **2017**, *8*, 14212−14222.

(17) Choi, H. J.; Suh, M. P. Dynamic and Redox Active Pillared Bilayer Open Framework : Single-Crystal-to-Single-Crystal Transformations upon Guest Removal, Guest Exchange, and Framework Oxidation. *J. Am. Chem. Soc.* **2004**, *126*, 15844−15851.

(18) Sava, D. F.; Rodriguez, M. A.; Chapman, K. W.; Chupas, P. J.; Greathouse, J. A.; Crozier, P. S.; Nenoff, T. M. Capture of Volatile Iodine, a Gaseous Fission Product, by Zeolitic Imidazolate Framework-8. *J. Am. Chem. Soc.* **2011**, *133*, 12398−12401.

(19) Sava, D. F.; Chapman, K. W.; Rodriguez, M. A.; Greathouse, J. A.; Crozier, P. S.; Zhao, H.; Chupas, P. J.; Nenoff, T. M. Competitive I_2 Sorption by Cu-BTC from Humid Gas Streams. *Chem. Mater.* **2013**, *25*, 2591−2596.

(20) Zhang, X.; da Silva, I.; Godfrey, H. G. W.; Callear, S. K.; Sapchenko, S. A.; Cheng, Y.; Vitorica-Yrezabal, I. J.; Frogley, M. D.; Cinque, G.; Tang, C. C.; et al. Confinement of Iodine Molecules into Triple-Helical Chains within Robust Metal−organic Frameworks. *J. Am. Chem. Soc.* **2017**, *139*, 16289−16296.

(21) Yao, Z.; Liu, C.-J.; Li, Y.; Jing, X.-D.; Yuan, Q. Helicity Analysis of Single, Double, and Triple Helical Iodine Chains inside Single-Walled Silicon Carbide Nanotubes. *Can. J. Phys.* **2017**, *95*, 731−737.

(22) Hu, X. L.; Sun, C. Y.; Qin, C.; Wang, X. L.; Wang, H. N.; Zhou, E. L.; Li, W. E.; Su, Z. M. Iodine-Templated Assembly of Unprecedented 3d-4f Metal-Organic Frameworks as Photocatalysts for Hydrogen Generation. *Chem. Commun.* **2013**, *49*, 3564−3566.

(23) Hsu, S. L.; Signorelli, A. J.; Pez, G. P.; Baughman, R. H. Highly Conducting Iodine Derivatives of Polyacetylene: Raman, XPS, and X-Ray Diffraction Studies. *J. Chem. Phys.* **1978**, *69*, 106−111.

(24) Talin, A. A.; Centrone, A.; Ford, A. C.; Foster, M. E.; Stavila, V.; Haney, P.; Kinney, R. A.; Szalai, V.; El Gabaly, F.; Yoon, H. P.; Léonard, F.; Allendorf, M. D. Tunable Electrical Conductivity in Metal-Organic Framework Thin-Film Devices. *Science* **2014**, *343*, 66−69.

(25) Schneider, C.; Ukaj, D.; Koerver, R.; Talin, A. A.; Kieslich, G.; Pujari, S. P.; Zuilhof, H.; Janek, J.; Allendorf, M. D.; Fischer, R. A. High Electrical Conductivity and High Porosity in a Guest@MOF Material: Evidence of TCNQ Ordering within Cu_3BTC_2micropores. *Chem. Sci.* **2018**, *9*, 7405−7412.

(26) Sun, L.; Campbell, M. G.; Dinca, M. Electrically Conductive Porous Metal-Organic Frameworks. *Angew. Chem., Int. Ed.* **2016**, *55*, 3566−3579.

(27) Hu, Y.-Q.; Li, M.-Q.; Wang, Y.; Zhang, T.; Liao, P.-Q.; Zheng, Z.; Chen, X.-M.; Zheng, Y.-Z. Direct Observation of Confined $I^-...I_2...I^-$ Interactions in a Metal-Organic Framework: Iodine Capture and Sensing. *Chem. - Eur. J.* **2017**, *23*, 8409−8413.

(28) Blake, A. J.; Li, W.-S.; Lippolis, V.; Parsons, S.; Radek, C.; Devillanova, F. A.; Gould, R. O.; Schroder, M. Template Self-Assembly of Polyiodide Networks. *Chem. Soc. Rev.* **1998**, *27*, 195−205.

(29) Yin, Z.; Wang, Q. X.; Zeng, M. H. Iodine Release and Recovery, Influence of Polyiodide Anions on Electrical Conductivity and

DOI: 10.1021/acs.inorgchem.9b02176
Inorg. Chem. 2019, 58, 14145−14150

Nonlinear Optical Activity in an Interdigitated and Interpenetrated Bipillared-Bilayer Metal-Organic Framework. *J. Am. Chem. Soc.* **2012**, *134*, 4857−4863.
(30) Li, G.-P.; Zhang, K.; Zhao, H.-Y.; Hou, L.; Wang, Y.-Y. Increased Electric Conductivity upon I2 Uptake and Gas Sorption in a Pillar-Layered Metal-Organic Framework. *ChemPlusChem* **2017**, *82*, 716−720.
(31) Yu, F.; Li, D. D.; Cheng, L.; Yin, Z.; Zeng, M. H.; Kurmoo, M. Porous Supramolecular Networks Constructed of One-Dimensional Metal-Organic Chains: Carbon Dioxide and Iodine Capture. *Inorg. Chem.* **2015**, *54*, 1655−1660.
(32) Hao, Z.; Yang, G.; Song, X.; Zhu, M.; Meng, X.; Zhao, S.; Song, S.; Zhang, H. A Europium(iii) Based Metal-Organic Framework: Bifunctional Properties Related to Sensing and Electronic Conductivity. *J. Mater. Chem. A* **2014**, *2*, 237−244.
(33) He, W. W.; Li, S. L.; Yang, G. S.; Lan, Y. Q.; Su, Z. M.; Fu, Q. Controllable Synthesis of a Non-Interpenetrating Microporous Metal-Organic Framework Based on Octahedral Cage-like Building Units for Highly Efficient Reversible Adsorption of Iodine. *Chem. Commun.* **2012**, *48*, 10001−10003.
(34) Chaudhari, A. K.; Mukherjee, S.; Nagarkar, S. S.; Joarder, B.; Ghosh, S. K. Bi-Porous Metal−organic Framework with Hydrophilic and Hydrophobic Channels: Selective Gas Sorption and Reversible Iodine Uptake Studies. *CrystEngComm* **2013**, *15*, 9465−9471.
(35) Gándara, F.; Uribe-Romo, F. J.; Britt, D. K.; Furukawa, H.; Lei, L.; Cheng, R.; Duan, X.; O'Keeffe, M.; Yaghi, O. M. Porous, Conductive Metal-Triazolates and Their Structural Elucidation by the Charge-Flipping Method. *Chem. - Eur. J.* **2012**, *18*, 10595−10601.

DOI: 10.1021/acs.inorgchem.9b02176
Inorg. Chem. 2019, 58, 14145−14150